Journal of Marine Research, 53, 403–431, 1995

Eddy statistics in the South Atlantic as derived from drifters drogued at 100 m

by H. Schäfer[1] and W. Krauss[1]

ABSTRACT

More than 130 satellite-tracked buoys drogued at 100 m depth have been deployed by us in the South Atlantic during the years 1990–1993 in an ongoing program. After eliminating those portions of the trajectories for which the drogue was off, Lagrangian eddy statistics are computed and compared to the results of a similar data set in the North Atlantic and to previous results for the South Atlantic. Regarding the relations based on Taylor's theory, no significant differences can be seen between the North and South Atlantic. The Lagrangian integral time scale is inversely proportional to the r.m.s.-velocity which implies that eddy diffusivity is directly proportional to the r.m.s.-velocity and not to the variance. Previous studies on that matter are most likely influenced by buoys which lost their drogue. Eddy length scale is constant with values of 37 km in zonal and 28 km in meridional direction, averaged over the entire Atlantic.

Eddy diffusivity varies between $2 \cdot 10^7$ and $8 \cdot 10^7$ cm^2/s, being smallest in the subtropics and highest in the Circumpolar Current. The proportionality to eddy velocity and a constant length scale opens the possibility to compute global distributions of eddy diffusivity from altimeter data.

1. Introduction

A large number of satellite-tracked buoys has been used during the last decades in order to study the large-scale current field and its fluctuations. However, the total data set is rather inhomogeneous, mainly due to different choices of drogue depth and unknown time of drogue losses.

The proper choice of drogue depth depends essentially on the scientific goals of the drift experiments, either

(i) to measure the actual flow within the mixed layer under given atmospheric conditions or

(ii) to gain as much information as possible on geostrophic currents, eddy kinetic energy and Lagrangian eddy statistics below the mixed layer, which is required in order to test numerical models.

1. Institut für Meereskunde, an der Universität Kiel, 24105 Kiel, Germany.

Currents in the mixed layer are a superposition of Ekman currents and geostrophic currents. Either one may be dominant depending on time and place. Currents derived from buoys drogued at 100 m depth are quasi-geostrophic currents modified by the drag of the Ekman currents on the buoy and on the tether.

The overwhelming part of drift data is either drogued within the mixed layer or undrogued.

McNally (1981) has shown for the eastern North Pacific that monthly averaged drift vectors (drogued at 30 m; NORPAX Data) mainly follow the mean isobars of the sea surface air pressure fields, at least during winter. This is interpreted as an Ekman deflection of about 30° to the right of the surface wind, assuming that the deflection of the surface wind to the left of the geostrophic wind is of the same order. The monthly averaged drift speeds in winter were 3.5 times those observed in summer. This increase coincided with a 5-time increase in the monthly averaged wind speed from summer to winter. On the average the drifters moved at a speed of 1.4% of the surface wind speed. Under low wind (late spring and summer) the drift direction was ill defined.

Based on a larger data set (75 drifters), McNally *et al.* (1983) supported the result that the trajectories in the mixed layer tend to follow time-averaged isobars rather than climatological geostrophy of the ocean.

During the anomalous winter 1982/83 over the northeastern Pacific, Emery *et al.* (1985) analyzed the tracks of 5 buoys drogued at 30 m. The monthly buoy and geostrophic wind directions were well correlated ($r \approx 0.9$); geostrophic wind speed to buoy speed showed correlations of $r \approx 0.7$. The buoys moved with 1.2% of the geostrophic wind speed. Emery *et al.* (1985) further cross-correlated the monthly mean buoy velocities with geostrophic ocean currents inferred from monthly mean dynamic heights (0/200 db). Geostrophic and buoy derived current speeds were almost uncorrelated ($r = -0.14$). The correlation coefficient between the direction of the mean monthly buoy velocities and the corresponding monthly geostrophic currents was $r = 0.09$.

If geostrophic currents strongly exceed the Ekman currents, the latter become only an additive component, except during severe storms. In the Gulf Stream (Richardson, 1983), the NAC near Flemish Cap and its associated eddy fields, geostrophic velocities often exceed Ekman currents by an order of magnitude, making the wind influence comparatively small. Outside strong currents and rigorous eddy fields there exists an apparent lack of correspondence between buoy trajectories drogued in the mixed layer and dynamic topography in mid- and high latitudes (Thomson *et al.*, 1990).

The worst contamination of drifter data results from unknown drogue loss. Only a few buoys were equipped with reliable drogue indicators in the 70's and early 80's. Nevertheless, buoys which lost their drogue have been widely used to describe the surface current field. Besides the fact that these buoys should be more exposed to the

wind drag—depending on the buoy type—most users of these buoys insist that they show similar drift behavior as buoys drogued within the mixed layer.

In the FGGE data set of the South Atlantic 55% of the buoys were deployed without drogues and approximately 39% with drogues initially attached at depths between 5 m and 30 m below the sea surface. For these buoys there is no information about drogue losses. Nevertheless, Garrett (1980) found no obvious difference between drogued and undrogued buoys. A similar result was reported by McNally (1981). Drifters drogued in 30 m moved with a speed of 1.4% of the surface wind speed, 36° to the right of the wind heading, while the undrogued drifters moved at a speed of 1.5% of the surface wind, 34° to the right of the wind heading. Generally, windage should increase with increasing ratio of buoy cross section to drogue cross section, reaching a maximum after drogue loss. Krauss *et al.* (1989) tested undrogued HERMES buoys with and without a 50 kg weight and found differences in drift velocities of 100% for wind velocities of 17 m s^{-1}.

The reliability of drifters drogued at 100 m depth has been under debate because windage and drag within the mixed layer should influence the drift performance (Poulain and Niiler, 1990). Drifters in the mixed layer have been calibrated for winds up to 12 m/s (e.g. Bitterman *et al.,* 1990), which does not cover the range in mid and high latitudes during the winter season. The performance of deep-drogued drifters has been mainly deduced from the consistency with flow patterns derived by other means. Colin de Verdiere (1983) came to the conclusion that buoys drogued at 100 m depth follow water motions with a r.m.s. precision of typically 15%. Booth (1988) estimated a slip velocity of less than $1.3 \cdot 10^{-3}$ of the surface wind velocity (< 1.3 cm/s for 10 m/s wind speed). Based on 8 drifters Krauss *et al.* (1989) showed that during the passage of a storm (reaching 25 m/s) the drift speed increased by 1.7 cm/s per 10 m/s increase in wind speed. Willebrand *et al.* (1990) compared geostrophic velocities derived from GEOSAT sea surface topography between the Azores, Newfoundland and Bermuda with geostrophic drift velocities from the stream function estimated from drifter velocities and obtained a regression $v_{\mathrm{Alt}} = 1.04\ (\pm 0.6) + 0.93\ (\pm 0.04)\ v_{\mathrm{Drift}}$; the correlation was $r = 0.81$.

The influence of currents in the mixed layer on deep-drogued drifters was recently discussed by Krauss (1995). Based on a data set from the North Sea it was shown that under winter conditions with severe storms the combined effect of wind drag and Ekman currents on buoys of the type used also in this study produced a slippage of less than 2 cm/s in 90% of all cases. Slippage of drifters drogued within the mixed layer was less than 1 cm/s in 95% of all cases. These results are based on the applicability of a quadratic drag law for the resistance of the system. With the slight reservation that under real storm conditions additional forces due to wave breaking may produce additional slippage, the flow patterns derived from deep-drogued drifters are consistent with quasigeostrophic current fields derived by other methods.

As mentioned above, the choice of drogue depth should be made according to the

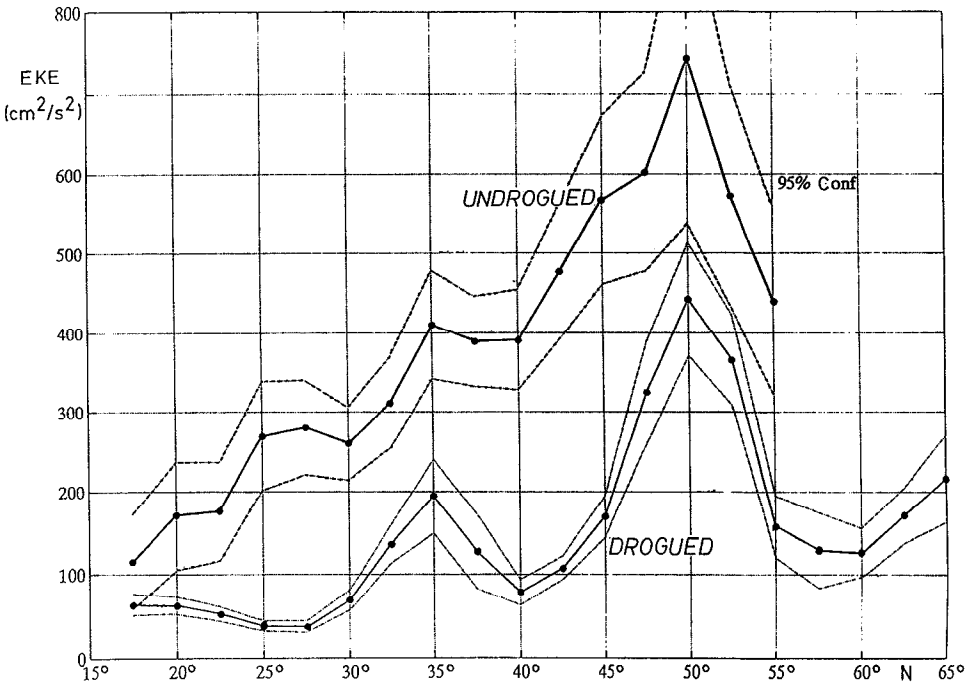

Figure 1. EKE along 30W between 15N and 65N in the North Atlantic (5° × 5° boxes) for buoys drogued at 100 m and undrogued ones.

scientific objectives and the area. As we are mainly interested in geostrophic currents and in Lagrangian properties of eddy fields that may be compared with the results of eddy resolving models, all buoys—except near the equator—were drogued below the seasonal thermocline, at 100 m depth. We are aware that during the winter season the mixed layer may reach even deeper in some areas. However, the direct influence of Ekman currents at that level should be small on average.

The IfM data set of the North Atlantic is based on HERMES buoys drogued at 100 m depth. 218 buoys were deployed during 1981–1989 yielding 70700 buoy days of data. By a careful analysis described by Brügge and Dengg (1991) buoys which lost their drogue have been separated from the drogued ones. The remaining data set served to compute the mean current field, eddy kinetic energies (EKE) and Lagrangian statistics (Krauss and Böning, 1987; Brügge, 1993) in the central and northern North Atlantic. The results obtained are supported by similar experiments with drifters drogued at 100 m by Booth (1988) in the northeastern North Atlantic and Thomson *et al.* (1990) in the North Pacific.

According to our results the rejection of undrogued buoys in the analysis of EKE or Lagrangian properties is essential. Figure 1 depicts EKE in the North Atlantic along 30W between 15N and 65N, based on 5° × 5° boxes, for drogued buoys and those which lost their drogue. EKE for undrogued buoys is 2–3 times higher.

Drogued buoys show that EKE is low at low latitudes, reaching a first maximum in the Azores Current at 35N and a second maximum in the North Atlantic Current near 50N. Undrogued buoys yield an entirely different distribution due to the wind influence.

So far, in the South Atlantic Ocean no systematic separation of drogued and undrogued buoys has been carried out. The results of Patterson (1985), Hofmann (1985), Johnson (1989)—among others—are based on the unseparated FGGE data set.

With the launch of SEASAT a new and independent data base became available for the computation of EKE (Cheney *et al.,* 1983). The first results for the South Atlantic showed that the EKE computed from FGGE-drifters was three times higher than that derived from altimeter data (Daniault and Ménard, 1985), which is consistent with Figure 1.

However, a striking difference between altimeter derived EKE and drifter EKE is the dependence of EKE on depth. Authors who derive EKE from altimeter data (both SEASAT and GEOSAT) conclude that higher EKE is found in deep water (>3 km) than in shallower areas (i.e. Sandwell and Zhang, 1989). Drifters do not support this result off the continental slope. Along the continental slope currents are known to be strongly steered by topography with less eddy shedding. In Figure 1 water depth exceeds 5000 m between 15N and 30N, where EKE is of the order 50 cm^2/s^2. North of 30N the distribution is mainly located along the Mid-Atlantic Ridge without any obvious influence of topography. The proposed topographic influence on EKE derived from altimeter data needs further interpretation.

Contrary to the North Atlantic, no deployments of drifters drogued below the mixed layer have been made in the South Atlantic before 1990. Lagrangian statistics for the South Atlantic based on FGGE and mixed layer drifters showed remarkable differences from deep-drogued drifters in the North Atlantic (Figueroa and Olson, 1989). In order to obtain better insight into the geostrophic circulation of the South Atlantic a program was started in 1990 to study the circulation in and around the subtropical gyre. A total of more than 200 buoys will be deployed until 1995. In the following section we describe the present data set (Section 2) and Lagrangian statistics for those areas where sufficient data are available (Sections 3 to 7). The results are discussed in Section 8.

2. Data set and methods

More than 130 buoys have been deployed in the South Atlantic between spring 1990 and 1993 in an ongoing program which aims to study the near surface geostrophic circulation. The areas of deployment are indicated in Figure 2 by the encircled numbers and are listed in Table 1. The drift direction becomes evident by comparing Figure 2 with the mean current vectors in Figure 5.

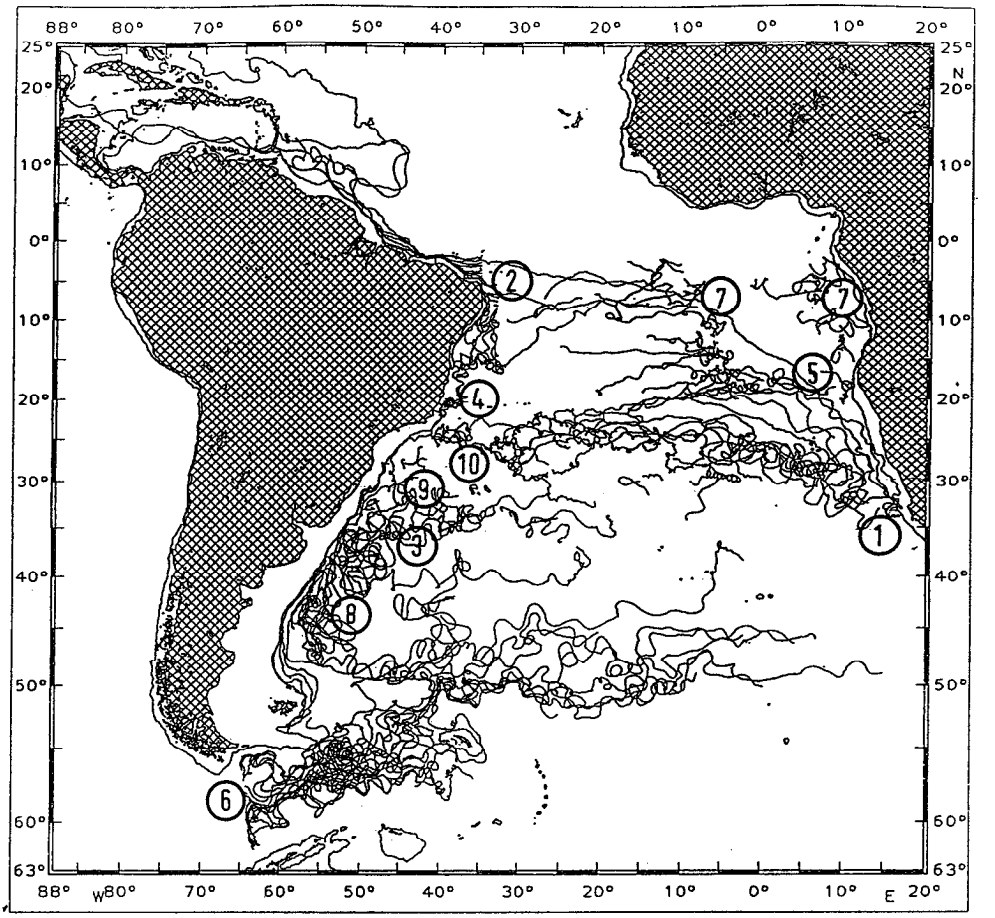

Figure 2. Trajectories of all buoys deployed in the South Atlantic. Additionally, the 1000 m isobath is shown. Encircled numbers: areas of deployment according to Table 1.

Table 1. Deployments in the South Atlantic

Time of deployment	Area	Number of buoys	Location in Figure 2
March 1990	Agulhas Leakage Area	14	1
October 1990	South Equatorial Current	20	2
January 1991	Brazil Current	20	3,4
March 1991	Benguela Current	10	5
December 1991	Ant. Circumpolar Current	20	6
January 1992	Benguela and Angola Current	30	7
September 1992	Falkland Current	8	8
December 1992	Central Subtropical Gyre	8	10

With the exception of the first 14 buoys, all buoys were of type SPAR. They have been built at the Institut für Meereskunde, Kiel, according to the specifications developed at AOML, Miami (Bitterman and Hansen, 1986).

The system consists of a spar buoy, which is a cylindrical tube of 2.60 m length and 11 cm diameter. Although the upper 60 cm are exposed to the wind, in practice this part is often submerged in rough sea. The cross areas of the buoy are 0.066 m^2 in air and 0.22 m^2 in water. A tether of 100 m length and 1.1 cm diameter, yielding a cross area of 1.1 m^2, connects the drogue with the buoy. The drogue is a holy sock of 10 m length and 1 m diameter, which gives a cross area of 10 m^2.

The first 14 buoys were of type HERMES. Their technical details are described by Krauss *et al.* (1989). The buoy is of conical form both above and below the sea surface. 1.1 m of its total length (2 m) are submerged. Cross areas above sea surface, below sea surface and the cross area of the window-shade drogue are .41 m^2, .43 m^2 and 15.6 m^2, respectively. All buoys have been deployed during cruises of *"Meteor"* and *"Polarstern"* in the South Atlantic.

The 14 HERMES buoys were launched in March 1990 west of Capetown in the Agulhas leakage area. Further deployments on the eastern side of the South Atlantic followed in March 1991 in the Benguela Current and in January 1992 in the Angola Current and along a section from 7S to 20S at 7W, which crosses the northeastern edge of the subtropical gyre and the Angola-Benguela Front. The bifurcation of the South Equatorial Current into the North Brazil Current and the Brazil Current was studied with another set of 20 buoys in October 1990. Further deployments in the Brazil Current followed in January 1991 (20 buoys). In the Falkland Current and the Falkland Confluence Zone 8 buoys were launched in September 1992 and 20 in the Drake Passage between Cape Horn and King George Island. The last 8 buoys used in this analysis were deployed in the central subtropical gyre in December 1992.

All buoys except those near the Brazil Current bifurcation were drogued at 100 m. The 20 buoys which were deployed near the eastern promontory of South America, Cabo de São Roque, had their drogue at 15 m depth in order to avoid the vertical shear of the equatorial current system.

Positions via ARGOS were received typically 6 times per day. Each time series was interpolated to 3 h equidistant intervals, using a Lagrangian 3 point interpolation routine. For the analysis of the data set, the time series were averaged over one day in order to remove the high frequency part of the fluctuations.

The elimination of undrogued buoys is relatively easy for the SPAR buoys due to the drogue indicator. This sensor is an electronic mercury switch which sends a signal if the buoy is tilted more than 40°, which is permanently the case after drogue loss.

For the older buoys (HERMES), a correlation method (Brügge and Dengg, 1991) was used, comparing drift and wind direction. As this method is reliable only for wind

speeds higher than a few knots, for these buoys, drogue loss could be determined only with a precision of some days, usually of weeks.

After elimination of those portions of the trajectories for which the drogue was off, 122 drifters with a total of 23775 buoy days remained (Fig. 3). The average drifting time was 190 days; some buoys were monitored just for a few days, the longest drifted for more than 20 months. One of the factors reducing buoy life was their recovery by fishermen, mainly on the South American shelf.

For statistical investigations it is necessary to average data of several buoys within geographical boxes. In selecting the box size, two different requirements should be fulfilled:

— each box should be as small as possible to reach a good spatial resolution and to obtain nearly homogeneous and stationary conditions as required in Taylor's theory;

— the number of data per box should be large enough to get significant results.

To find an optimal box size for statistical computations we adopt a method developed by Brügge (1993) for the North Atlantic data set. According to Riser and Rossby (1983) the errors of both the mean value $\bar{u}$ and the r.m.s.-velocity $\sqrt{\overline{u'^2}}$ are dependent on $\sqrt{\overline{u'^2}}/\sqrt{N_m}$ where N_m is the number of independent samples, which is related to the Lagrangian integral time scale T by $N_m = N/2T$, N being the number of data points. For a 95% confidence level we have

$$\bar{u} \pm \frac{2\sqrt{\overline{u'^2}}}{\sqrt{N_m}}, \sqrt{\overline{u'^2}} \pm \frac{2 \cdot \sqrt{\overline{u'^2}}}{\sqrt{2 \cdot N_m}}. \tag{1}$$

Thus, the errors are not only dependent on the number of independent data but also on the eddy kinetic energy (EKE) in the box, i.e. different box sizes can be chosen for different areas.

Tests both in the North and South Atlantic show that the 95% confidence limit is a rather strict measure: mean values and variance converge much faster in most cases, which allows further reduction of the box size.

The method applied is demonstrated in Figure 4 for the boxes AGU 1 and BRA 5. As the sequence of data is unimportant for computing mean values etc., the data in each box have been rearranged ten times in a random fashion. Figure 4 depicts the cumulative mean as function of time for these sequences. This clearly shows that a stable mean value is reached faster than given by the (arbitrarily chosen) 95% limit (broken line). As a practical measure we define mean values and variances to be stable if the deviations from the final values are less than 2.5% (dashed-dotted line).

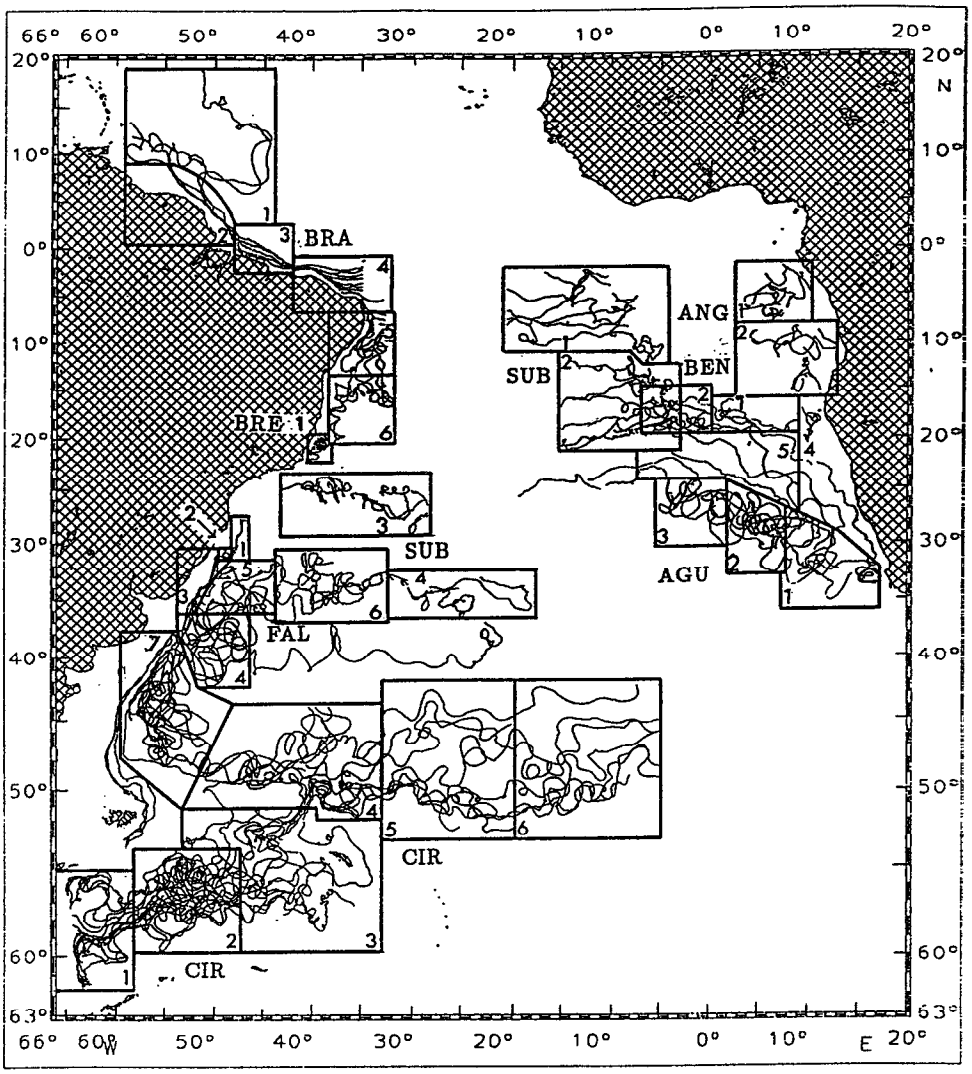

Figure 3. Remaining data set of drogued drifters used for this analysis. Additionally the chosen boxes are shown.

Thus, size and shape of a box were chosen in such a way as to fulfill this criterion. According to this method, the box size is not only determined by the number of data but also by the local flow characteristics. Because some boxes are rather small or passed with high speed, the number of data points per box varies from 68 to 2517, with an average of 665 days. The final boxes are indicated in Figure 3. The following

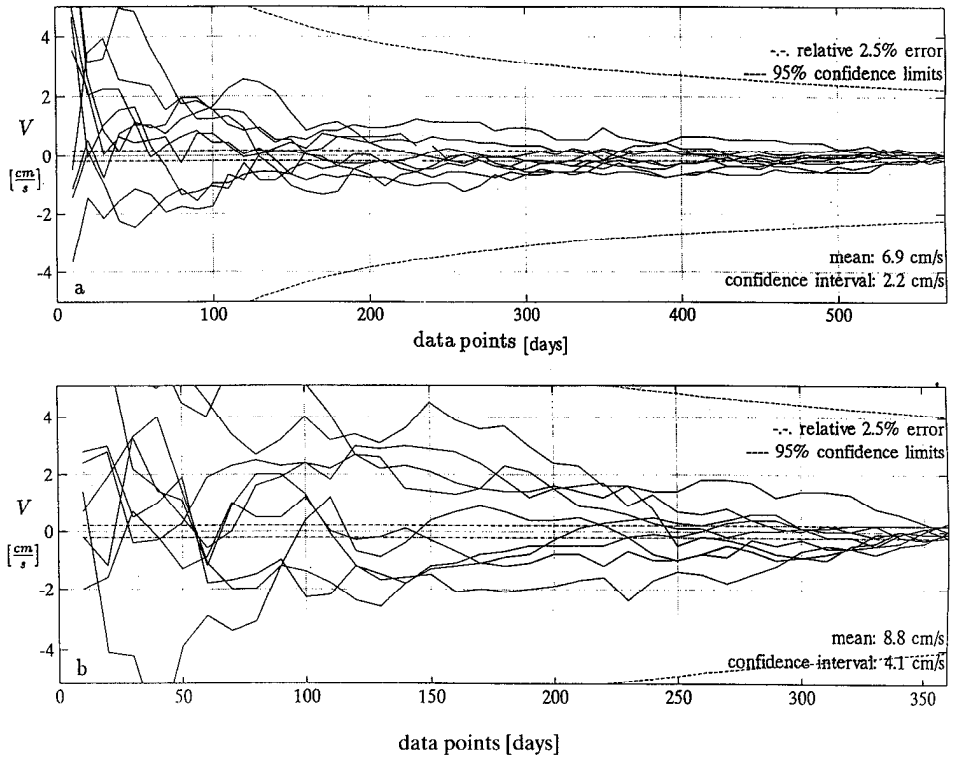

Figure 4. Cumulative mean of 10 different randomly arranged velocities minus the final mean for boxes AGU 1 (a) and BRA 5 (b) as function of data points. Dashed lines: 95% confidence limits, dashed-dotted lines: relative 2.5% error.

abbreviations are used:

AGU 1–5: Agulhas leakage area of the Benguela Current
BEN 1–2: Benguela Current region
ANG 1–2: Angola Current region
BRA 1–6: North Brazil Current and Brazil Current
BRE 1 : Brazil Current eddy
FAL 1–7: Falkland Current and Falkland Confluence Zone
CIR 1–6: Antarctic Circumpolar Current
SUB 1–4: Subtropical Gyre of the South Atlantic.

3. Mean values, r.m.s.-velocities and Eddy kinetic energy

A detailed description of the upper level geostrophic circulation of the South Atlantic Ocean has been given by Peterson and Stramma (1991). Their schematic picture is shown in Figure 5 by thin lines. According to that the center of the

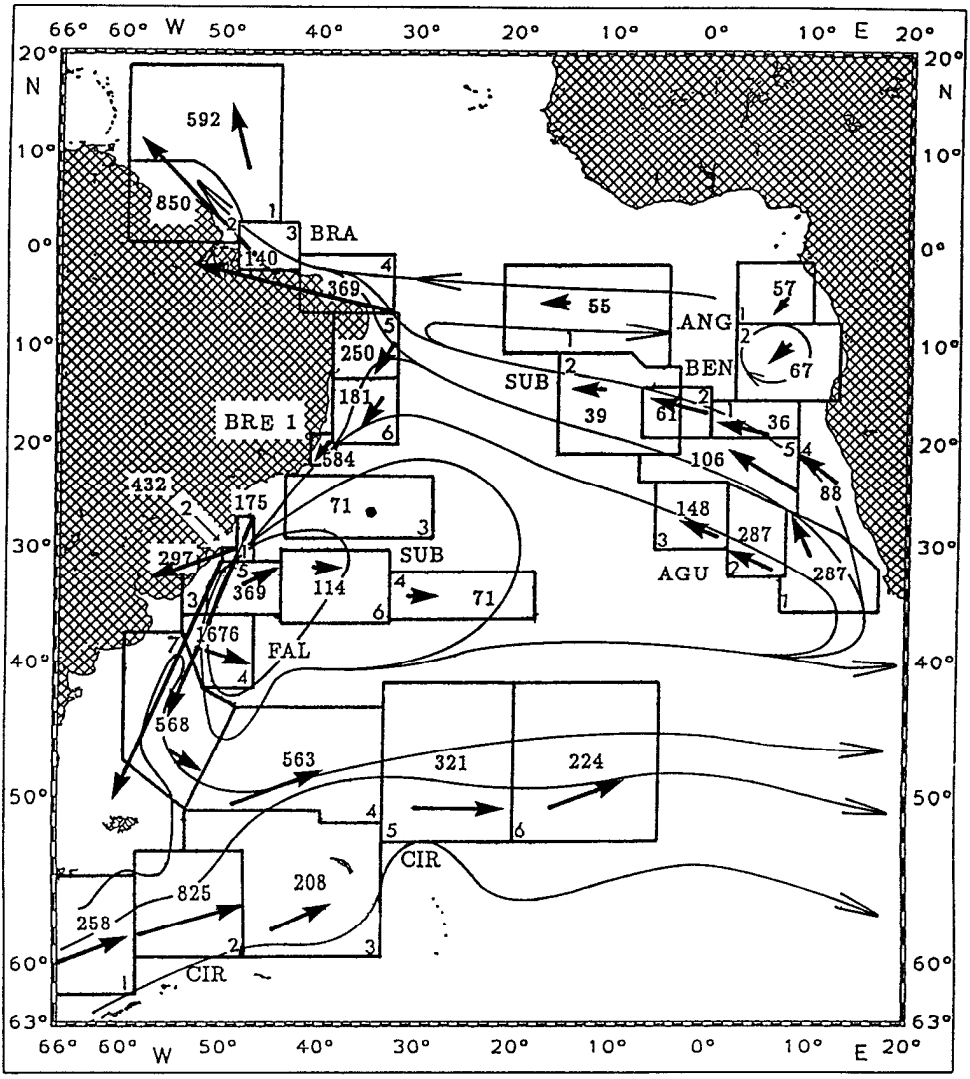

Figure 5. Schematic current picture of the South Atlantic according to Peterson and Stramma (1991) and distribution of the eddy kinetic energy according to Table 3. Also shown are mean currents according to Table 2 (arrows).

subtropical anticyclonic gyre is located at about 35S, 45W. The gyre extends in a triangular shape across the entire South Atlantic. On the African side, the flow around this gyre consists of the Benguela Current, which continues into the South Equatorial Current across the Atlantic. Near the Brazilian Coast it divides into the strong Brazilian Current, which crosses the Equator and the weak Brazil Current, which intensifies on its way south. A further branch emerges as South Equatorial

Counter Current along 8S toward the east and is embedded into the South Equatorial Current. In the Angola Basin weak circulation is associated with the Angola Dome.

On the south western side of the subtropical gyre the Falkland Current penetrates as far north as 40S resulting in the Confluence Zone when it meets with the warm Brazil Current. The eastward flow along 40S is known as South Atlantic Current and the currents south of it form the Antarctic Circumpolar Current.

Most of the information on these currents stems from ship drift observations and geostrophic calculations. The boxes described in the previous section have not been chosen to obtain a broad coverage of the current branches but to compute stable r.m.s. velocities for the description of the eddy field. The mean current field is presently under calculation by nudging the drift velocities into a numerical model. In Table 2 and Figure 5 the mean velocities serve only as reference velocities for the r.m.s.-values. $\bar{u}$ and $\sqrt{\overline{u'^2}}$ are given according to Eq. 1. Compared to the schematic picture of Peterson and Stramma (Fig. 5) the center of the subtropical gyre appears further north in box SUB 3 (mean velocities $\bar{u} = .1, \bar{v} = .0$ cm/s) with easterly return flow from the Confluence Zone already between 30S and 35S. Also note (Fig. 3) that drifters in the Falkland Current mainly leave the Confluence Zone toward the southeast, turning eastward between 45S and 50S. This is consistent with the schematic geostrophic pattern (Fig. 5), whereas the SOS drifters of the mixed layer (Fugueroa and Olson, 1989) leave the Confluence Zone between 35S and 40S. This may be a systematic difference between the two levels.

The region southwest of Africa was divided into seven boxes. The southernmost are AGU 1–3 in the Benguela Current. They show the highest current variability in the eastern South Atlantic, mainly caused by eddies of the Agulhas leakage area. Box AGU 4 contains drifters near the shelf edge where upwelling plays a dominant role. BEN 1 and 2 are located in the northern region of the Benguela Current which explains the mainly westerly flow. The mean current speed decreases from 11 cm/s in the southern Benguela Current (AGU 5) to 5 cm/s in the northern part (BEN 2). Eddy velocities drop from 24 cm/s to 9 cm/s. Near 10S, in the Angola Current, two boxes (ANG 1, 2) represent a region with very weak mean currents but a variability of nearly 8 cm/s. At the northern edge of the South Equatorial Current, areas SUB 1, 2 show a distinct westerly current of more than 4 cm/s without any meridional mean velocity. Obviously, the South Equatorial Current dominates the Counter Current. Eddy velocities remain at 7 cm/s. Similar values for the r.m.s.-velocity hold in the central boxes of the subtropical gyre (SUB 3 and 4) with zero mean velocity in SUB 3. The region of the North Brazil Current is divided into four boxes. Note that these drifters are drogued at 15 m depth. The northern-most box (BRA 1) shows high variabilities caused by temporal changes of the mean flow, not due to high eddy activities. This box is located in an area where seasonally reversible currents were observed due to the retroflection of the North Brazil Current into the North

Table 2. Mean currents and r.m.s.-velocities in the boxes shown in Figure 3.

Region	Buoys numbers	Buoy days	$\overline{U}$ cm/s	$\Delta\overline{U}$ 95%	$\overline{V}$ cm/s	$\Delta\overline{V}$ 95%	U' cm/s	$\Delta U'$ 95%	V' cm/s	$\Delta V'$ 95%
AGU 1	9	579	−3.3	±1.8	6.1	±2.0	18.6	±1.3	15.1	±1.4
AGU 2	9	658	−6.2	±1.5	1.7	±2.2	15.4	±1.1	18.4	±1.6
AGU 3	5	540	−3.8	±1.9	2.2	±1.7	11.9	±1.3	12.5	±1.2
AGU 4	5	458	−4.2	±2.0	4.8	±2.1	8.6	±1.4	10.1	±1.5
AGU 5	6	484	−10.4	±1.8	5.7	±1.7	10.6	±1.3	10.0	±1.2
BEN 1	6	499	−5.5	±1.2	1.6	±1.3	6.2	±0.9	5.8	±0.9
BEN 2	5	663	−5.1	±1.5	1.3	±0.8	8.4	±1.0	7.2	±0.6
ANG 1	5	751	0.3	±1.4	−0.2	±1.1	8.1	±1.0	6.9	±0.8
ANG 2	6	703	−0.8	±1.6	−1.0	±1.4	7.9	±1.1	8.5	±1.0
SUB 1	11	2013	−4.1	±0.9	0.0	±0.7	8.1	±0.6	6.6	±0.5
SUB 2	14	2577	−4.3	±0.6	−0.2	±0.5	6.7	±0.4	5.9	±0.4
SUB 3	5	949	0.1	±1.3	0.0	±1.0	8.5	±0.9	8.4	±0.7
SUB 4	4	559	3.2	±1.9	−0.2	±1.3	9.1	±1.4	7.8	±0.9
BRA 1	5	369	−1.4	±5.6	8.6	±3.7	25.0	±4.0	23.7	±2.6
BRA 2	5	70	−48.5	±6.5	63.8	±7.5	30.7	±4.6	27.5	±5.3
BRA 3	7	309	−14.4	±2.8	8.2	±2.1	12.5	±2.0	11.1	±1.5
BRA 4	13	242	−32.3	±4.0	7.2	±3.2	23.1	±2.8	14.3	±2.3
BRA 5	9	368	−1.9	±2.3	−3.9	±3.4	13.5	±1.6	17.8	±2.4
BRA 6	4	516	−2.4	±1.6	−3.7	±2.1	13.1	±1.1	13.8	±1.5
BRE 1	8	185	1.5	±2.9	−1.7	±3.1	24.6	±2.0	23.8	±2.2
FAL 1	9	109	−10.4	±1.9	−30.5	±2.7	13.0	±1.4	13.4	±1.9
FAL 2	9	68	−11.9	±5.7	−5.6	±4.5	22.5	±4.0	18.9	±3.2
FAL 3	8	121	−17.5	±2.8	−36.4	±3.4	12.3	±1.9	21.1	±2.4
FAL 4	7	330	5.9	±3.8	−2.0	±3.3	37.1	±2.7	44.4	±2.3
FAL 5	7	394	4.6	±2.8	4.1	±2.1	19.7	±2.0	18.7	±1.5
FAL 6	3	932	2.7	±1.6	−0.3	±1.2	10.3	±1.1	11.0	±0.9
FAL 7	5	884	3.3	±2.0	−2.7	±2.8	20.2	±1.4	27.0	±2.0
CIR 1	19	864	8.4	±1.7	3.4	±1.5	16.4	±1.2	15.8	±1.1
CIR 2	20	785	15.6	±2.6	6.1	±2.0	27.3	±1.9	30.0	±1.4
CIR 3	15	1146	6.1	±1.5	3.8	±0.9	14.8	±1.0	14.1	±0.7
CIR 4	13	869	11.8	±2.3	4.6	±1.5	24.4	±1.6	23.0	±1.0
CIR 5	9	731	12.9	±1.9	0.4	±1.5	17.3	±1.3	18.5	±1.1
CIR 6	7	819	10.4	±1.8	2.7	±1.4	15.2	±1.2	14.8	±1.0

Equatorial Counter Current during fall (Richardson and Reverdin, 1987). In the other three boxes, the highest mean speeds with 80 cm/s (not shown as arrow in Fig. 5) were measured. The narrow current is strongly controlled by topography as evident from the straight trajectories in Figure 3. Besides that, r.m.s. speed still varies between 20 and 40 cm/s. The southward flowing Brazil Current separates at 7S and is represented by BRA 5,6. In addition a coastal counter current is found, tracked by two buoys. The Brazil Current is very weak between 7S and 20S (4 cm/s) and is dominated by the r.m.s.-velocities of approximately 15 cm/s. Box BRE 1 describes a cyclonic eddy near Victoria, Brazil, leading to high r.m.s. values. This eddy had a

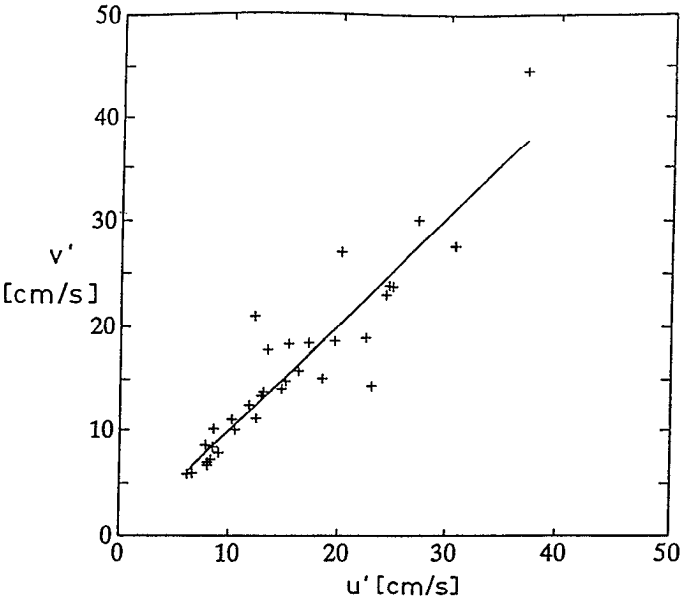

Figure 6. r.m.s.-velocity components of all boxes, v' versus u'.

diameter of 100 km and moved slowly during the observation period of 55 days, probably due to the influence of the Abrolhos Bank and some seamounts farther south. A detailed description of this eddy is given by Schmid *et al.* (1995).

More to the center of the subtropical gyre are the boxes SUB 3,4 showing small mean and r.m.s.-velocities. The rest of the boxes are located near the Brazil-Falkland Confluence Zone. FAL 1–3 represent the narrow Brazil Current before reaching the Confluence Zone, including an eddy with high mean velocities. The Brazil Current in these boxes increases to 40 cm/s. FAL 4–7 cover areas of the Confluence Zone with strong variability, leading to the highest r.m.s. values of all boxes up to $u' = 37$ cm/s and $v' = 44$ cm/s. To the east, the flow in the South Atlantic Current is almost zonal with 12 cm/s, combined with decreasing variability (CIR 4–6). Three boxes (CIR 1–3) represent the Circumpolar Current in the Drake Passage and the Scotia Sea. This area has high r.m.s. velocities comparable with those in the Brazil-Falkland Confluence Zone and a relatively high eastward mean velocity of 16 cm/s. Box CIR 2 in the central Scotia Sea shows very high variability up to 40 cm/s. With the exception of the topographically sterred North Brazil Current and the southern Brazil Current r.m.s.-velocities exceed the mean velocities considerably. In Figure 6 r.m.s.-velocities of all boxes are depicted, showing that eddy velocities are isotropic. The regression is $v' = -0.10 + 1.01\,u'$, the correlation being $r = 0.92$.

EKE-values for all boxes based on the r.m.s.-velocities are also shown in Figure 5. The high energy area of the Agulhas reflection area is not covered by our data. In the Agulhas leakage area values of slightly less than 300 cm^2/s^2 are reached. This energy

level is strongly reduced further north in the Benguela Current and toward the West-African shelf. Typical values in the South Equatorial Current and in the Angola Current are about 50 cm^2/s^2, in the central subtropical gyre the values are even less.

The western boundary currents in the South Atlantic Ocean show much less EKE than in the North Atlantic. Values are typically between 200–400 cm^2/s^2, probably due to the topographic steering of the North Brazil and the Brazil Current. The Falkland Current reaches more than 500 cm^2/s^2 with a maximum in the confluence zone, where the Brazil and the Falkland Current separate from the continental slope. The maximum of 1600 cm^2/s^2 in the confluence zone decreases rapidly in the South Atlantic Current farther east.

In the Antarctic Circumpolar Current maximum values of more than 800 cm^2/s^2 are reached in the Scotian Sea. These values also decrease rapidly to 200–300 cm^2/s^2 farther east.

EKE distributions as derived from FGGE drifters show generally higher values except in the Circumpolar Current (Piola *et al.,* 1987). This holds especially in the central subtopical gyre and at low latitudes. Based on the 14 drifters of the Southern Ocean Studies, Garraffo *et al.* (1992) obtained 100 cm^2/s^2 in the central South Atlantic between 30S and 50S. These values are also higher than ours in low latitudes but lower in the Circumpolar Current.

Values of 1600 cm^2/s^2 in the confluence zone have also been obtained from GEOSAT data (Provost and Le Traon, 1993). Our values support their result that the meridional variance is larger than the zonal one in the confluence zone.

4. Prerequisite for the validity of Taylor's theory

In the subsequent sections we shall test the applicability of Taylor's theory on homogeneous isotropic turbulence (Taylor, 1921) to the drifter data. Taylor's theory describes particle dispersion and Lagrangian diffusivity in a homogeneous isotropic turbulent field. In the ocean the turbulent velocity components u', v' are mainly due to eddies and meanders, if high frequency fluctuations like inertial and tidal waves are removed. This can approximately be achieved by using daily averages of the velocities. However, at low latitudes, inertial waves may still contaminate the data.

The decomposition into mean and fluctuating quantities, $u = \bar{u} + u'$, is only correct if the motion of the center of gravity of the drifters in a box is properly described by the mean motion. This can be checked by plotting the displacement of the center of gravity of the drifters of each box as function of time in comparison with $x = \bar{u}t$ etc. As in the North Atlantic (Colin de Verdière, 1983) the data show that this holds generally for less than 60 days. Special care is required in areas with current reversals. In a northward flowing current like the Falkland Current which reverses its direction in the confluence area and turns back toward the south before turning eastward (FAL 7), nearly all of its speed appears as r.m.s.-velocity. Such a

Table 3. Boxes in which the prerequisites of Taylor's theory are not fulfilled.

Box	Component	Reason
AGU4	x, y	Flow is steered by topography in water of less than 1000 m
BRA 2	x, y	"
BRA 3	x, y	"
BRA 4	x, y	"
FAL 1	x, y	"
FAL 2	x, y	"
FAL 3	x, y	"
BRE 1	x, y	Isolated eddy fixed by topography
BRA 1	x, y	Outside the area of the South Atlantic
BRA 5	y	Reversal of the meridional current component, appearing as v'
FAL 7	y	"

reversal occurs also in the Brazil Current (BRA 5), where part of the drifters first move southward and later return back to their origin in a coastal current. These areas have to be excluded from the analysis.

Violation of isotropy occurs mainly in narrow western boundary currents with strong shear and in topographically steered currents. In these cases free turbulence on the eddy scale is largely suppressed as seen by inspection of the trajectories in Figure 3 along the Patagonian continental slope (Falkland Current), in the North Brazil Current and along the continental slope in the southern Brazil Current. Shallow topography further induces spacial fluctuations on topographic scales, that are not related to free turbulence. For these reasons the boxes listed in Table 3 have not been included in the subsequent analysis. This reduces the number of boxes to 24 for the x-component, 22 for the y-component.

5. Integral time scale and length scale

The Lagrangian integral time scale plays a central role in Taylor's theory, which has proved to be a reliable concept for the description of eddy statistics in the ocean. This time scale can be calculated in two different ways. One possibility is to use the autocorrelation function. For real data, the autocorrelation function often does not approach zero, either due to a bad separation of the mean current from the fluctuations or because of oscillatory components like Rossby waves, which falsify the integral time scale. By convention, the time scale is generally chosen as the integral from zero to the time of the first zero crossing. Consequently, the integral time scales can appear larger than in reality due to the neglection of negative lobes of the autocorrelation function, also in cases where they are real. An alternative approach is to use the dependence of dispersion on the integral time scale in the random walk regime. This random walk regime begins about 10 days after the initial dispersion

and is characterized by a reduced increase in dispersion, proportional to the square root of time, or in squared form

$$\overline{x'^2} = 2 \cdot \overline{u'^2} \cdot t \cdot T. \tag{2}$$

T stands for the Lagrangian time scale, which can be computed for each box from x' and u' according to this relation.

The procedure is as follows: The data base for the statistical description of diffusion can be considerably increased by making use of homogeneity and stationarity of the flow within each box. We used the same method as outlined by Colin de Verdière (1983), splitting the time series of the drifters in each box into a number of series by restarting the series after a multiple of 10 days. These 10 days are in all cases longer than the decorrelation time of the drifters. This method breaks down if the assumption of homogeneity is violated, but the same holds for the Taylor theorem. Tests with slightly different restarting lags show little influence on the results.

Figure 7 depicts some dispersion curves in x- and y-direction as full and dotted lines, respectively. Eq. (2) states that under the assumption of the validity of the Taylor theory there exists a range (t_1, t_2), in which $\overline{x'^2}$ can be approximated by a straight line. In a log–log plot (Fig. 7) the inclination of this line is fixed, its intercept with the ordinate is dependent on $\overline{u'^2}$ and T. Subjective judgement has been used to approximately determine the range (t_1, t_2) over which the approximation holds. This range is shown in Figure 7 by the full and broken straight lines. The integral time scale was computed as mean value

$$T_m = \frac{1}{2\overline{u'^2}} \left[\frac{\overline{x'^2(t)}}{t} \right]_m ,$$

for this range.

Obviously, there is some arbitrariness in fixing the range (t_1, t_2), which influences T_m and the standard deviation. However, the same holds if the autocorrelation function is used for determining T.

The examples depicted in Figure 7 are chosen to show the large variety of problems involved. Boxes AGU 3 and CIR 6 are rather clearcut cases. BEN 2 and BRA 6 give shorter ranges for the zonal and larger ranges for the meridional dispersion. The most difficult case is FAL 4 in the confluence zone, where the range 10–20 days could also have been chosen. Instead of .9 ± .1 d and .5 ± .1 d for the zonal and meridional time scales, respectively, we then would have arrived at 1.8 ± 1.1 d and 1.4 ± .3 d. In all other cases it is mainly the standard deviation which is influenced by changing the length of the interval; box CIR 3 is a characteristic example.

The integral time scales, their standard deviation, and the chosen time range

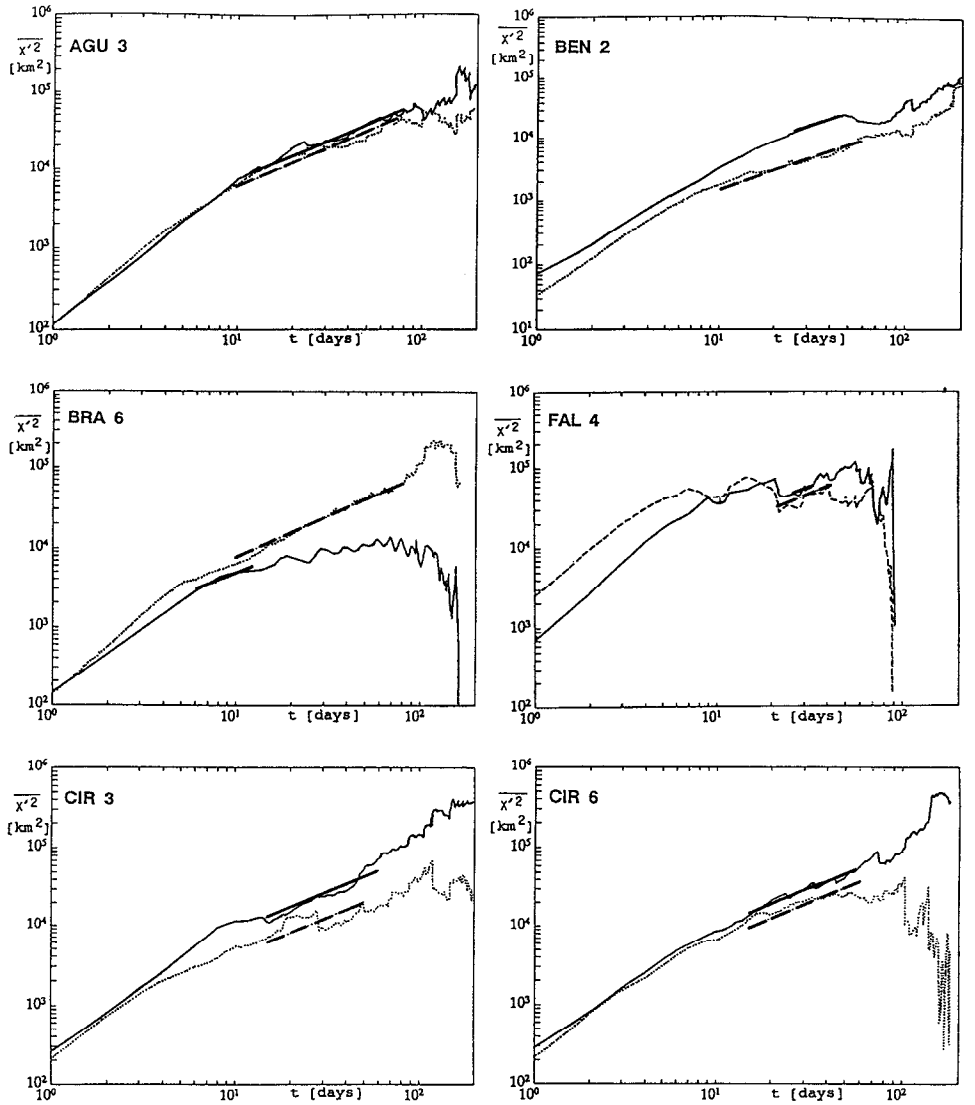

Figure 7. Square of dispersion for zonal (full line) and meridional component (dotted line) and theoretical dispersion from the Taylor theory for the random walk regime.

(t_1, t_2) are shown in Table 4 for all boxes except those excluded according to Table 3. Areas with a narrow flow have the smallest time scales (BRA 2, FAL 1–3 not shown in Table 4). In other regions, the integral time scale grows with decreasing variability. Good examples are boxes AGU 1–3, where the variability decreases while the time scale grows with increasing distance from the Agulhas leakage region. The same pattern was observed for boxes FAL 4–6 as well as for boxes CIR 4–6, while the areas

Table 4. r.m.s.-velocities u', v', time range of the random walk regime (t_1, t_2), Lagrangian integral time scales T_1, T_2, length scales L_1, L_2 and eddy diffusivities K_1, K_2

	Scales and coefficients									
Region	u' cm/s	v' cm/s	$(t_1, t_2)_1$ days	$(t_1, t_2)_2$ days	$T_1 \pm \Delta T$ days	$T_2 \pm \Delta T$ days	L_1 km	L_2 km	$K_1 \cdot 10^7$ cm²/s	$K_2 \cdot 10^7$ cm²/s
AGU1	18.6	15.1	10,60	10,50	1.3 ± 0.4	2.4 ± 0.2	22	32	4.0	4.8
AGU2	15.4	18.4	10,80	10,40	1.6 ± 0.4	2.4 ± 0.6	21	38	3.2	6.9
AGU3	11.9	12.5	20,80	10,80	3.4 ± 0.4	2.5 ± 0.4	35	27	4.2	3.3
AGU5	10.6	10.0	12,38	12,38	3.5 ± 0.3	3.6 ± 0.3	32	32	3.4	3.2
BEN 1	6.2	5.8	10,55	10,15	4.9 ± 0.9	6.3 ± 0.3	26	32	1.6	1.8
BEN 2	8.4	7.2	25,40	10,60	5.0 ± 0.3	2.3 ± 0.2	37	14	3.1	1.0
ANG1	8.1	6.9	15,80	15,50	5.4 ± 1.2	4.5 ± 0.3	38	27	3.1	1.9
ANG2	7.9	8.5	15,60	15,60	7.0 ± 1.0	4.6 ± 0.4	48	33	3.8	2.8
SUB 1	8.1	6.6	15,50	15,60	6.1 ± 1.0	5.3 ± 0.5	43	30	3.5	2.0
SUB 2	6.7	5.9	15,60	15,60	4.7 ± 0.2	5.3 ± 0.5	27	27	1.8	1.6
SUB 3	8.5	8.4	15,50	15,40	5.6 ± 0.6	3.7 ± 0.2	41	27	3.5	2.2
SUB 4	9.1	7.8	10,40	15,50	6.4 ± 2.3	4.0 ± 0.7	50	27	4.5	2.1
BRA 5	13.5		10,22		2.7 ± 0.2		31		4.2	
BRA 6	13.1	13.8	6,12	10,80	1.9 ± 0.1	2.8 ± 0.2	21	34	2.8	4.7
FAL 4	37.1	44.4	25,34	22,41	0.9 ± 0.1	0.5 ± 0.1	27	17	10.2	7.7
FAL 5	19.7	18.7	10,80	10,90	2.0 ± 0.2	1.2 ± 0.3	34	20	6.6	3.7
FAL 6	10.3	11.0	15,35	15,35	5.4 ± 0.7	2.9 ± 0.4	49	27	5.0	3.0
FAL 7	20.2		15,40		2.1 ± 0.3		37		7.6	
CIR 1	16.4	15.8	15,50	10,30	2.4 ± 0.4	2.0 ± 0.4	33	26	5.4	4.2
CIR 2	27.3	30.0	15,40	15,90	1.8 ± 0.3	0.9 ± 0.2	42	22	11.5	6.7
CIR 3	14.8	14.1	15,60	15,50	2.8 ± 0.5	1.3 ± 0.4	36	15	5.3	2.2
CIR 4	24.4	23.0	15,50	15,40	2.0 ± 0.2	0.9 ± 0.2	41	17	10.1	3.9
CIR 5	17.3	18.5	15,60	15,60	2.2 ± 0.2	1.2 ± 0.2	32	19	5.6	3.5
CIR 6	15.2	14.8	15,60	15,60	2.7 ± 0.2	1.8 ± 0.4	36	23	5.4	3.4

in the middle of the subtropical gyre (SUB 3, 4) and those at the northern edge show low variability and therefore large time scales. In order to demonstrate that the time scale is not very different, even for those boxes in which the prerequisites of Taylor's theory may be violated, we first show the integral time scale for all boxes (including those of Table 3) in Figure 8.

Comparing time scales with r.m.s.-velocities, an inverse proportionality between T and $\sqrt{u'^2}$ is obvious. Drifters drogued at 15 m depth are given in parentheses. Note that these do not significantly differ from those drogued at 100 m. The least square fit is taken from Figure 9. This curve, the relation $T \sim 1/u'$, is based on the data of the South Atlantic (+ symbols only), excluding the boxes of Table 3. Also included in this figure are the results for the North Atlantic according to Krauss and Böning (1987), given by the symbol x, and those of Figueroa and Olson (1989) for the South Atlantic

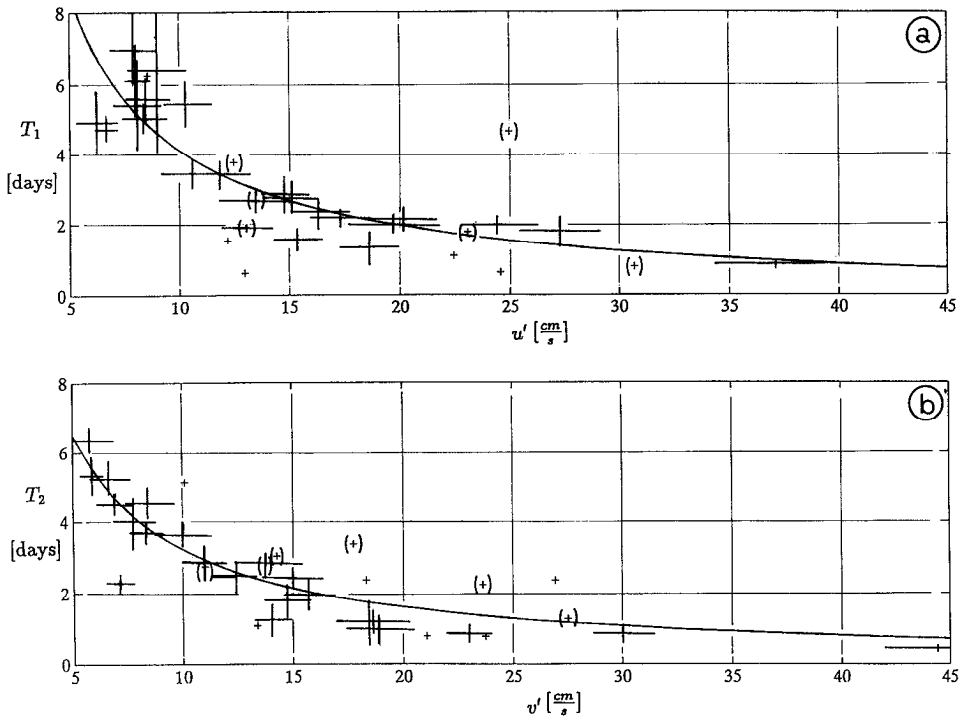

Figure 8. Integral time scales as a function of r.m.s. velocities for all boxes and least square fit according to Figure 9. Values in parentheses are from drifters drogued at 15 m depth. (a) zonal, (b) meridional. Large crosses show error bars with respect to u' and T, respectively. Small crosses are values according to Table 3, which are omitted in the subsequent figures.

(circles). The relations shown in Figure 9 are

$$T_1 = -0.1 + \frac{42.9}{\sqrt{u'^2}}, \; T_2 = -0.4 + \frac{36.6}{\sqrt{v'^2}} \tag{3}$$

for the zonal and the meridional component with correlation coefficients 0.86 and 0.97, respectively. For convenience, T is given in days but $\sqrt{u'^2}$ in cm/s.

A comparison with Figueroa and Olson's time scales of the South Atlantic shows large deviations in the zonal time scale, which corresponds to the dominant wind direction. For a box in the area of FAL 4 and 5, they found time scales of 4.4 and 2.3 days at r.m.s.-velocities of 28 and 32 cm/s, much larger than our values. In another box which could be compared with box FAL 6, Figueroa and Olson derived time scales of 5.9 and 2.0 days at r.m.s.-velocities of 17 and 18 cm/s. This again shows, as already outlined with respect to Figure 1, that drifters in the mixed layer, especially if contaminated by unknown drogue losses, do not characterize the geostrophic flow field. Apart from the SOS drifters the data set used by Figueroa and Olson also

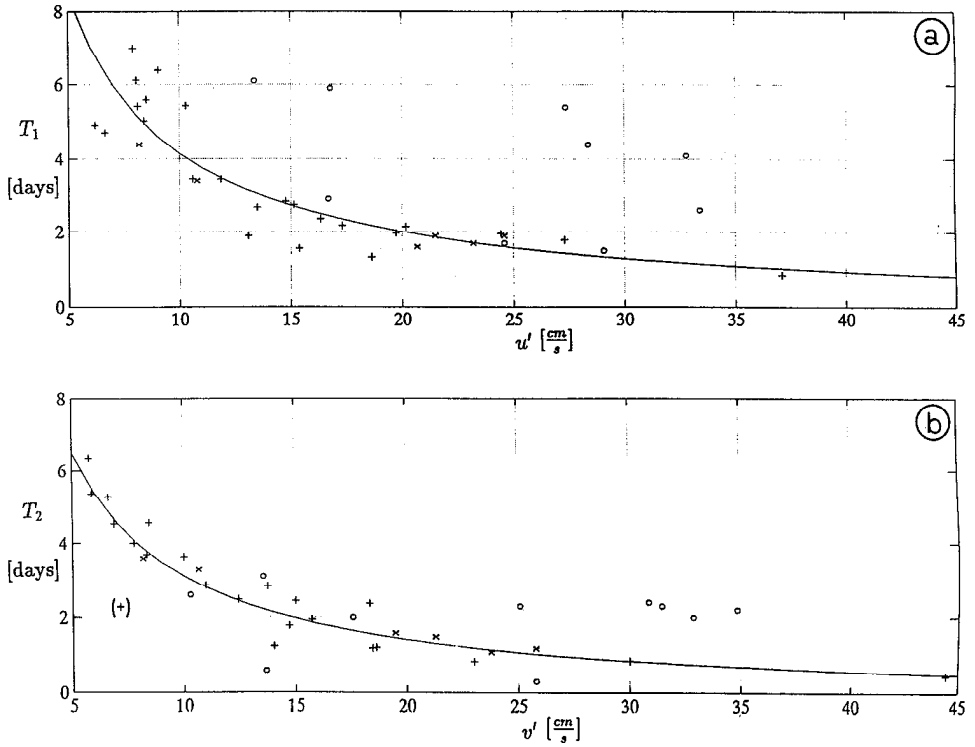

Figure 9. Like Figure 8, but only for those areas where free turbulence can develop. Included are values of Krauss and Böning (1987) for the North Atlantic (symbol x). Also shown are the values of Figueroa and Olson (1989) for the South Atlantic (circles).

contains buoys from the FGGE data set. These buoys were deployed for meteorological purposes and were of different shape; in addition, most of them had no drogue, thus they may be under strong wind influence. The other part of the data set came from the Southern Ocean Studies; these buoys were originally equipped with a drogue in the mixed layer, with unknown date of drogue loss. This might explain the larger time scales, especially in zonal direction. Different from our observations, the data of Figueroa and Olson do not show a systematic relation between integral time scales and r.m.s.-velocities.

Contrary to that, the values for the North Atlantic (Krauss and Böning, 1987) fit very well into our results (Fig. 9). The inverse proportionality between integral time scale and r.m.s.-velocity holds for the entire Atlantic Ocean. This is important for the discussion of eddy diffusivities.

In the analysis given above, T_2 for box BEN 2 has been omitted. This data point is shown in parentheses in Figure 9 and the consecutive Figures. The Angola-Benguela Front is located in this area (Peterson and Stramma, 1991), separating the Angola Dome from the subtropical gyre. As seen from Table 4, BEN 2 shows an unusually

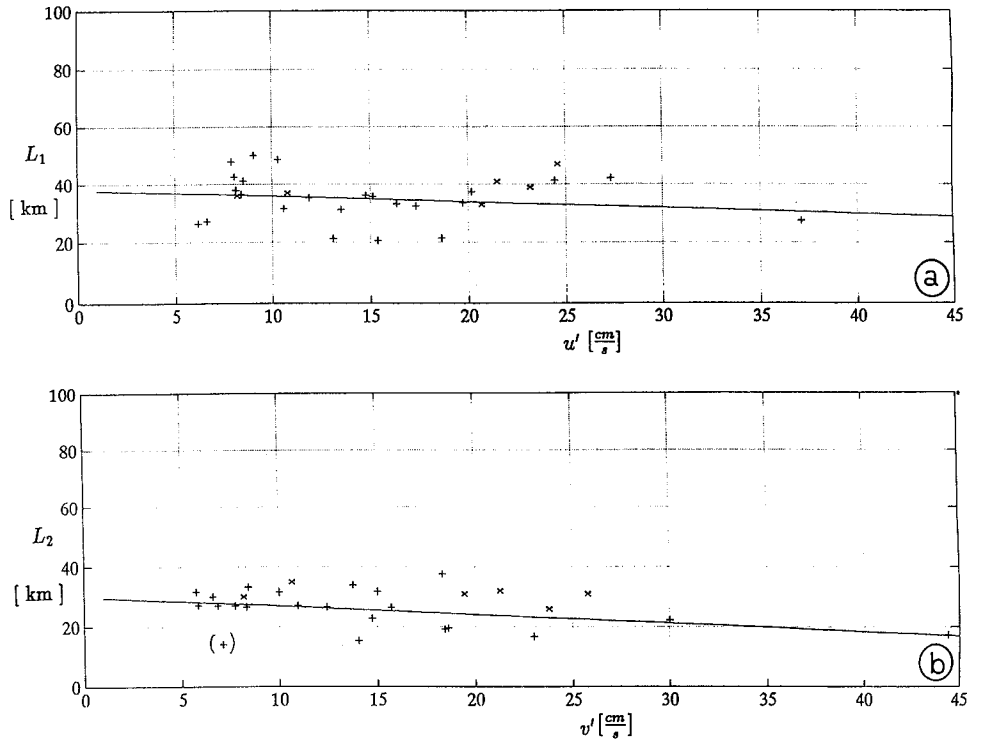

Figure 10. Integral length scales as a function of r.m.s. velocities and least square fit. Symbol x represents values of Krauss and Böning (1987) for the North Atlantic (a) zonal, (b) meridional.

low integral time scale T_2 (2.3 days) and correspondingly a very short length scale L_2 (14 km) and low eddy diffusivity k_{22} ($1.0 \cdot 10^7$ cm^2/s) for $v' = 7.2$ cm/s. Inspection of the trajectories in that area reveals that the buoys perform a large number of rather small scale loops, which start at the mean position of that front. It seems that small scale eddies develop at the front which are transported west by the mean flow and which do not have the characteristics of eddies elsewhere in the South Atlantic. This area surely needs further investigations. Further note that $T_2 > T_1$ in the Agulhas leakage area (AGU 1 and AGU 2), contrary to most other boxes. This is due to a larger dispersion in y-direction, probably an effect of the Agulhas rings.

Based on the integral time scale, an integral length scale can be computed according to $L = T \cdot \sqrt{u'^2}$, which describes the distance after which two velocity observations become uncorrelated, i.e. the distance passed after an integral time scale. These values are also given in Table 4. If $T \sim 1/u'$ would fit perfectly, L would be a constant. From Figure 10 it can be seen that this assumption is roughly fulfilled. Note that the slight inclination of the line is mainly caused by the last value on the right of Figure 10, which stems from the uncertain value of box FAL 4. The average

length scale in the South Atlantic is 35 km zonally and 26 km meridionally. These mean length scales agree very well with those of the North Atlantic, where 39 and 31 kilometers were calculated on average. As time scale is unisotropic, length scale and eddy diffusivity must have the same characteristics.

6. Single particle dispersion

Single particle dispersion allows an important test for the validity of Taylor's theory. From the result in the North Atlantic we expect:

(i) a rapid increase of the dispersion after the release of the buoys (initial dispersion) up to considerably less than 10 days, $\overline{x'^2} = \overline{u'^2}\, t^2$

(ii) a reduced increase after this time (random walk regime), $\overline{x'^2} = 2\overline{u'^2}\, Tt$, established after 10 days on average

(iii) a regime with strong random fluctuations as a consequence of less data points during the last days, but otherwise a tendency for a saturation level.

This saturation level would be an upper bound for the horizontal dispersion. Because homogeneity and stationarity are the main premises for Taylor's theory, unstable mean velocities will falsify the results.

Figure 11 depicts the initial dispersion for some boxes. Indicated are the lines of theoretical dispersion and the observed ones. During the first 2–3 days Taylor's relation holds for all boxes, except FAL 4, the confluence zone. After about 10–15 days, most buoys have reached the random walk regime (Fig. 7 and Table 4). The distance from the origin ranges from 50–100 km. In this random walk regime, Taylor's theory predicts a linear relationship between the square of dispersion and time. In the log–log plots of Figure 7, this behavior is also seen up to a time where the data base becomes too small. This is generally the case after 80 days. Summarizing these results: a reasonably good agreement between Taylor's theory and our observations was found for the whole South Atlantic, where the prerequisites of the theory are given and a sufficient amount of data is available. Outside of topographically steered currents (Table 3), the Falkland–Brazil Confluence Zone appears as an area where most likely the prerequisites of Taylor's theory are violated.

7. Diffusivity

The Lagrangian diffusivity is generally obtained by differentiation of dispersion with respect to time. However, this procedure is very sensitive to small variations of the dispersion. To avoid the influence of these variations, the Taylor theorem is used for the calculation of diffusivity. For time scales longer than 10 days, this leads to the relation $K = \overline{u'^2} \cdot T$, which is constant. These values are given in Table 4. They correspond to those in the North Atlantic. With growing r.m.s.-velocities, diffusivity

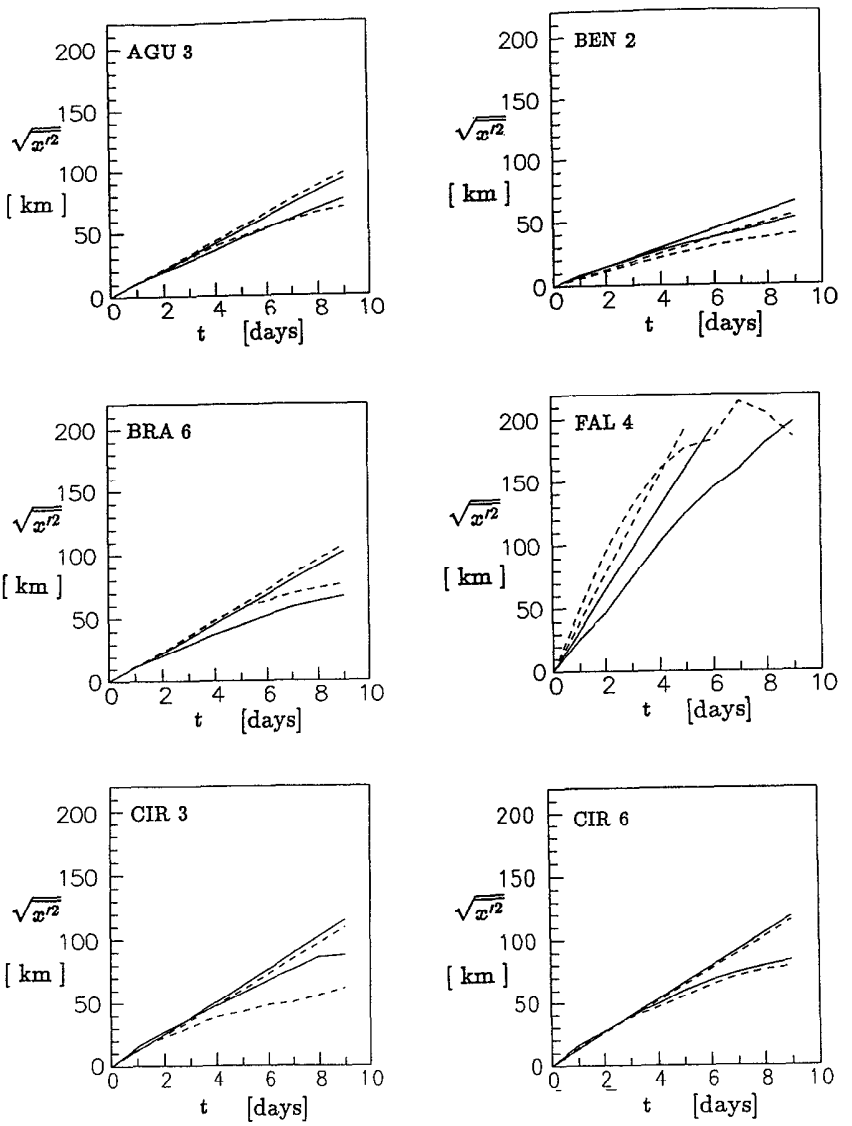

Figure 11. First 10 days of dispersion in zonal (full line) and meridional direction (broken line). Straight lines are calculated from the Taylor Theory. Shown are a few typical boxes.

rises linearly for both the zonal and the meridional component (Fig. 12). The corresponding relations are $K_1 = (0.5 + 0.31 \cdot u') \cdot 10^7$ zonally and $K_2 = (1.2 + 0.16 \cdot v') \cdot 10^7$ meridionally, with a correlation coefficient of 0.88 and 0.86, respectively. Note the anisotropy, yielding much larger values for zonal diffusivity. Figure 12 additionally includes the values of Krauss and Böning (1987) (symbol x).

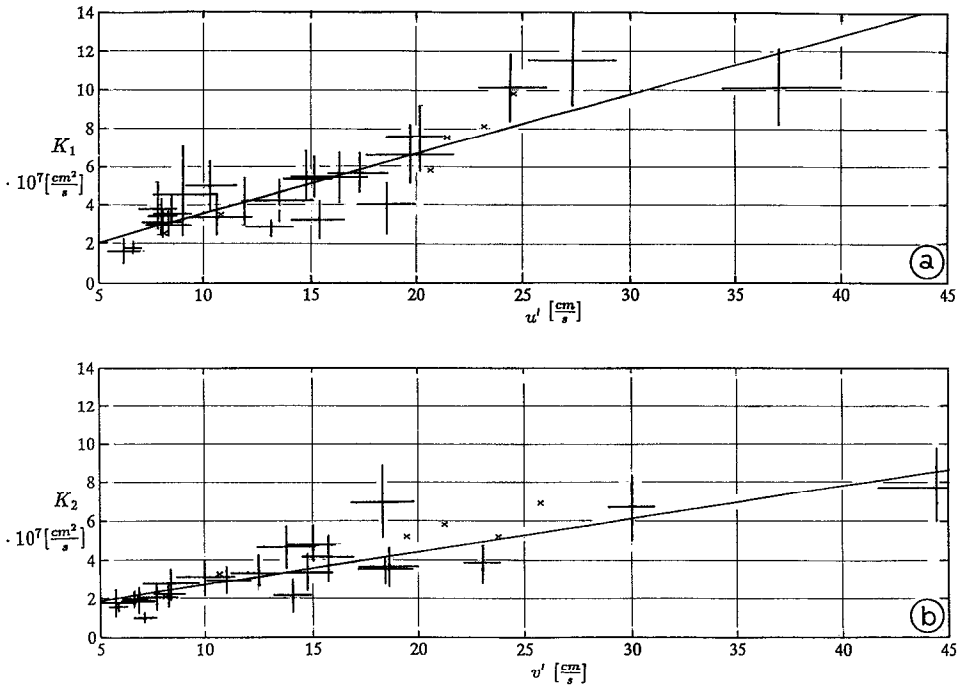

Figure 12. Diffusivities in zonal (a) and meridional direction (b) as function of r.m.s.-velocity. Straight lines: least square fit. Symbol x denotes values for the North Atlantic according to Krauss and Böning (1987). Crosses show error bars with respect to u' and K. Mean errors for K are computed from those of u' and T according to Tables 2 and 4.

Colin de Verdiére (1983) and Booth (1988) found diffusivities of the same order in the eastern North Atlantic. The same holds for the results of Thomson *et al.* (1990) from the North Pacific. Contrary to that, Figueroa and Olson (1989) found values which are much higher than ours. Figueroa and Olson further compared the dependence of diffusivity both on velocity variance and on r.m.s.-velocities and found no significant differences between both relations. Indeed, our data also allow a linear fit to both. However, assuming a linear dependence of eddy diffusivity on the variance $\overline{u'^2}$ implies that the integral time scale is not dependent on u'. Figure 9 clearly shows that this does not hold for drifters drogued at 100 m depth. A constant value could be used for the data of Figueroa and Olson (circles in Fig. 9), because their u', v' are all larger than 10 cm/s, probably due to drogue problems.

In Figure 13 we depict the meridional distribution of eddy diffusivity. As in the North Atlantic, diffusivity increases linearly with latitude from $2 \cdot 10^7$ cm^2/s in the subtropics to $8 \cdot 10^7$ and $5 \cdot 10^7$ cm^2/s at 60S for zonal and meridional directions, respectively.

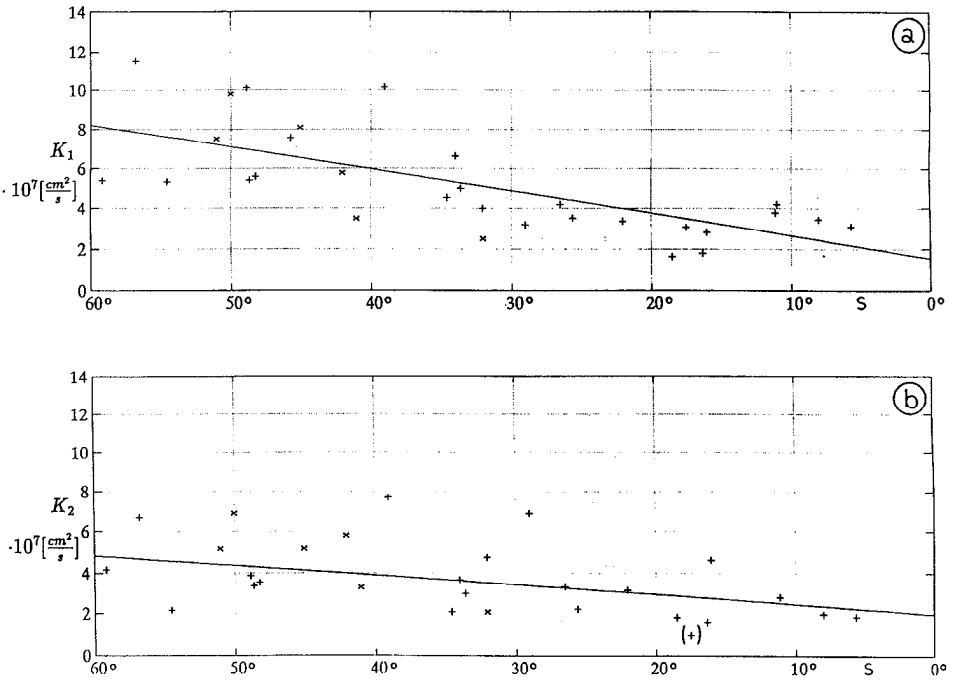

Figure 13. Same as Figure 12 as a function of latitude instead of r.m.s.-velocities.

8. Summary and conclusions

Combined with the results from the North Atlantic, 122 drifters in the South Atlantic drogued beneath the mixed layer at 100 m depth give a unique picture of the Lagrangian eddy statistics in the entire Atlantic Ocean. Results from the northern North Pacific Ocean (Thomson *et al.,* 1990) fit well into this concept. As all parameters in Taylor's theory, integral time scale, integral length scale, particle dispersion and eddy diffusivity, depend on the eddy kinetic energy, correct determination of ensemble mean velocity and the deviations u', v' are crucial in testing this theory. For the North Atlantic it has been shown (Fig. 1) that undrogued drifters yield EKE's two to three times higher than those drogued at 100 m depth. Therefore, drifters which lost their drogue have to be removed from the data set prior to any statistical analysis. The separation of undrogued buoys from drogued ones is most easily done if the buoys are equipped with drogue indicators. A reliable separation is also possible for deep-drogued buoys by using distinct criteria like response to the actual wind etc. (Brügge and Dengg, 1991). However, this method becomes difficult for drifters in strong currents like the Gulf Stream, where the geostrophic flow is highly dominant.

There is no doubt that the homogeneity assumption in Taylor's theory is strongly violated in intensive current regimes with strong shear. Nevertheless, there emerges

a consistent picture of the mesoscale dispersion in the upper ocean. As in the North Atlantic, the integral time scale is inversely proportional to the r.m.s.-velocity of the eddy field. This implies, if Taylor's theory holds, that the Lagrangian integral length scale must be constant and that eddy diffusivity must grow linearly with the r.m.s.-velocity. As EKE increases outside the western boundary currents and their associated eddy fields from the subtropics toward higher latitudes, eddy diffusivity also increases. At 10S EKE is typically 50 cm^2/s^2 and eddy diffusivity amounts to $2 \cdot 10^7$ cm^2/s. EKE increases to 200–300 cm^2/s^2 at 60S and correspondingly, diffusivities to $8 \cdot 10^7$ cm^2/s and $5 \cdot 10^7$ cm^2/s for zonal and meridional direction, respectively.

Whereas the r.m.s.-velocity is isotropic, the Lagrangian integral time scale is not, being larger in zonal than in meridional direction. Due to the relations in the Taylor theory, length scale and diffusivity must show the same anisotropy. The enhancement of particle dispersion in zonal direction is probably due to the β-effect.

The striking similarity of the results for the South Atlantic with a previous analysis for the North Atlantic allows the conclusion that the derived properties are generally valid in the upper-ocean geostrophic eddy field. Thus it is possible to parameterize eddy diffusivity according to $K_{ii} = \sqrt{\overline{u_i'^2}} L_i$, where L_i is the Lagrangian length scale, which characterizes the "mixing length." For the North Atlantic, Krauss and Böning (1987) derived average values $L_1 = 39$ km, $L_2 = 31$. For the South Atlantic we obtain $L_1 = 35$ km, $L_2 = 26$ km. Thus, appropriate values, which can be used ocean-wide, may be $L_1 = 37$ km, $L_2 = 28$ km. With eddy kinetic energy becoming more and more available on a world-wide basis by satellite altimeters, eddy diffusivity is no longer an arbitrary quantity for the upper ocean beneath the mixed layer. However, its depth dependence remains an open question. Both RAFOS floats and numerical models (Böning, 1988) indicate e.g. a systematic depth dependence of the mixing length in the North Atlantic subtropical gyre. The increasing number of floats used in the deep ocean may shed further light on the problem.

REFERENCES

Bitterman, D. S. and D. V. Hansen. 1986. The design of a low cost tropical drifter buoy. Paper presented at Marine Data Systems International Symposium, Mar. Technol. Soc., New Orleans, L.A. April 30 to May 2, 1986.

Bitterman, D. S., P. Niiler, Y. Aoustin and A. du Chaffaut. 1990. Drift buoy—intercomparison test results, NOAA Data Rep. ERL AOML-17, 1–52.

Böning, C. W. 1988. Characteristics of particle dispersion in the North Atlantic: An alternative interpretation of SOFAR float results. Deep-Sea Res., *35,* 1379–1385.

Booth, D. A. 1988. Horizontal dispersion in the northeast Atlantic, Deep-Sea Res., *35,* 1937–1951.

Brügge, B. 1993. Über die Eigenschaften der oberflächennahen Zirkulation im zentralen Nordatlantik. Diss., Kiel, 131 pp.

Brügge, B. and J. Dengg. 1991. Differences in drift behavior between drogued and undrogued satellite-tracked drifting buoys. J. Geophys. Res., *96*(C4), 7249–7263.

Cheney, R. E., J. G. Marsh and B. D. Beckley. 1983. Global mesoscale variability from collinear tracks of SEASAT altimeter data. J. Geophys. Res., *88*(C7), 4343–4354.

Colin de Verdière, A. 1983. Lagrangian eddy statistics from surface drifters in the eastern North Atlantic. J. Mar. Res., *41,* 375–398.

Daniault, N. and Y. Ménard. 1985. Eddy kinetic energy distribution in the southern ocean from altimetry and FGGE drifting buoys. J. Geophys. Res., *90*(C6), 11877–11889.

Emery, W. J., T. C. Royer and R. W. Reynolds. 1985. The anomalous tracks of North Pacific drifting buoys 1981 to 1983. Deep-Sea Res., *32,* 315–347.

Figueroa, H. A. and D. B. Olson. 1989. Lagrangian statistics in the South Atlantic as derived from SOS and FGGE drifters. J. Mar. Res., *47,* 525–546.

Garraffo, Z., S. L. Garzoli, W. Haxby and D. Olson. 1992. Analysis of a general circulation model 2. Distribution of kinetic energy in the South Atlantic and Kuroshio/Oyashio Systems. J. Geophys. Res., *97*(C12), 20139–20153.

Garrett, J. F. 1980. Availability of the FGGE drifting buoy system data set. Deep-Sea Res., Part A, *27,* 1083–1086.

Hofmann, E. E. 1985. The large-scale horizontal structure of the Antarctic Circumpolar Current from FGGE drifters. J. Geophys. Res., *90*(C4), 7087–7097.

Johnson, M. A. 1989. Southern ocean surface characteristics from FGGE buoys. J. Phys. Oceanogr., *19,* 696–705.

Krauss, W. 1995. On the slippage of deep-drogued drifters. J. Geophys. Res., (submitted).

Krauss, W. and C. W. Böning. 1987. Lagrangian properties of eddy fields in the northern North Atlantic as deduced from satellite-tracked buoys. J. Mar. Res., *45,* 259–291.

Krauss, W., J. Dengg and H.-H. Hinrichsen. 1989. The response of drifting buoys to currents and wind. J. Geophys. Res., *94*(C3), 3201–3210.

McNally, G. J. 1981. Satellite-tracked drift buoy observations of the near-surface flow in the eastern mid-latitude North Pacific. J. Geophys. Res., *86*(C9), 8022–8030.

McNally, G. J., W. C. Patzert, A. D. Kirwan, Jr. and A. C. Vastano. 1983. The near surface circulation of the North Pacific using satellite tracked drifting buoys. J. Geophys. Res., *88*(C12), 7507–7518.

Patterson, S. L. 1985. Surface circulation and kinetic energy distributions in the Southern Hemisphere Oceans from FGGE drifting buoys. J. Phys. Oceanogr., *19,* 865–884.

Peterson, R. G. and L. Stramma. 1991. Upper-level circulation in the South Atlantic Ocean. Prog. Oceanogr., *26,* 1–73.

Piola, A. R., H. A. Figueroa and A. A. Bianchi. 1987. Some aspects of the surface circulation south of 20° revealed by First GARP Global Experiment drifters. J. Geophys. Res., *92,* 5101–5114.

Poulain, P.-M. and P. P. Niiler. 1990. Comment on "The Response of drifting buoys to currents and wind," by Krauss *et al.* J. Geophys. Res., *95*(C1), 797–799.

Provost, C. and P.-Y. LeTraon. 1993. Spatial and temporal scales in altimetric variability in the Brazil-Malvinas Current confluence region: dominance of the semiannual period and large spatial scales. J. Geophys. Res., *98*(C10), 18037–18051.

Richardson, P. L. 1983. Eddy kinetic energy in the North Atlantic from surface drifters. J. Geophys. Res., *88*(C7), 4355–4367.

Richardson, P.L. and G. Reverdin. 1987. Seasonal cycle of velocity in the Atlantic North Equatorial Counter current as measured by surface drifters, current meters and ship drifts. J. Geophys. Res., *92,* 3691–3708.

Riser, S. C. and H. T. Rossby. 1983. Quasi-Lagrangian structure and variability of the subtropical western North Atlantic circulation. J. Mar. Res., *41,* 127–162.

Sandwell, D. T. and B. Zhang, 1989. Global mesoscale variability from the GEOSAT exact repeat mission: correlation with ocean depth. J. Geophys. Res., *94*(C12), 17971–17984.

Schmid, C., H. Schäfer, G. Podestá and W. Zenk. 1995. The Vitória eddy and its relation to the Brazil Current. J. Phys. Oceanogr., (submitted).

Taylor, G. I. 1921. Diffusion by continuous movement. Proc. London Math. Soc. Ser. A, *20,* 196–221.

Thomson, R. E., P. H. LeBlond and W. J. Emery. 1990. Analysis of deep-drogued satellite-tracked drifter measurements in the northeast Pacific. Atmosphere-Ocean, *28,* 409–443.

Willebrand, J., R. H. Käse, D. Stammer, H.-H. Hinrichsen and W. Krauss. 1990. Verification of GEOSAT sea surface topography in the Gulf Stream extension with surface drifting buoys and hydrographic measurements. J. Geophys. Res., *95*(C3), 3007–3014.

Received *15 March, 1994;* revised: *31 January, 1995.*